High Resolution Topography of the Southern San Andreas Fault from Painted Canyon to Bombay Beach, California, USA

Michael P. Bunds[1], Chelsea Scott[2], Brigham Whitney[1], and Vicki J.C. Lee[3]

[1] Department of Earth Science, Utah Valley University, 800 West University Parkway, Orem, UT 84058
[2] School of Earth and Space Exploration, Arizona State University, Tempe, AZ 85287
[3] Department of Geosciences, Virginia Polytechnic Institute, Blacksburg, VA 24061

For additional information, please contact Michael Bunds (michael.bunds@uvu.edu).

DOI: https://doi.org/10.5069/G94M92RG

Introduction

This document is a technical overview of a new high-resolution topography and orthomosaic dataset that covers ~40 km of the Coachella section of the Southern San Andreas Fault, California, USA, from Painted Canyon to Bombay Beach (Figures 1 and 2). We used structure-from-motion (SfM) processing to generate the dataset from optical photographs taken with a small uncrewed aerial system (sUAS) and differential global navigation satellite system (dGNSS) measurements made in February, 2020. In this overview, we discuss the motivation and purpose of our dataset and provide a description of the data products, the field data collection, data processing, and uncertainty in the topographic model. The data set is available free-to-public from OpenTopography (https://opentopography.org). We request that use of the dataset is acknowledged with authorship information and the DOI.

Background and Motivation

The Coachella section of the Southern San Andreas has a high likelihood of hosting a major, surface-rupturing earthquake in the coming decades (e.g., UCERF3, 2017) and therefore is of great interest to the earthquake science community. We were motivated to collect an open SfM-based topography dataset because of the scientific interest in the area, the ground surface is well-resolved with SfM techniques due to the lack of vegetation, and our new dataset complements the B4 lidar data collected in 2005 (Bevis and Hudnut, 2005). Our effort also serves as a test-run for response to a future surface-rupturing earthquake as we have refined a rapid field data collection and processing approach. We envisage that the data will be a valuable resource for research and education in earthquake geology, geomorphology, and geomorphic change.

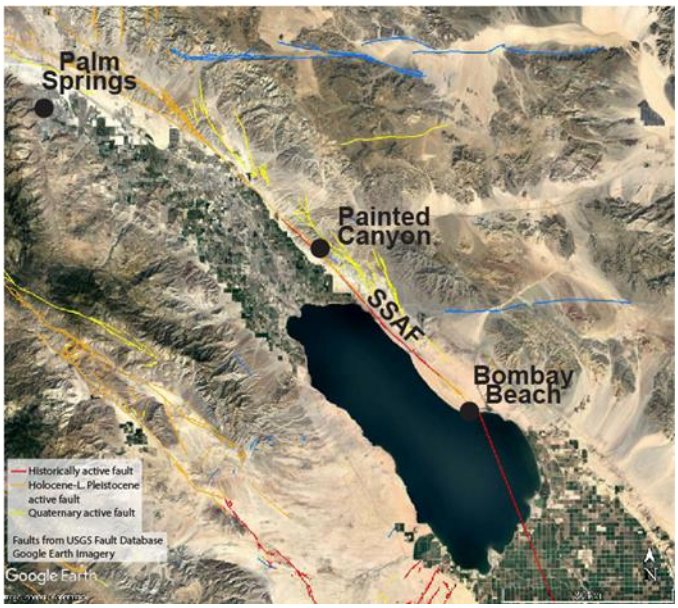

Figure 1. Regional map; our new dataset covers the Southern San Andreas Fault (SAF) from Painted Canyon to Bombay Beach.

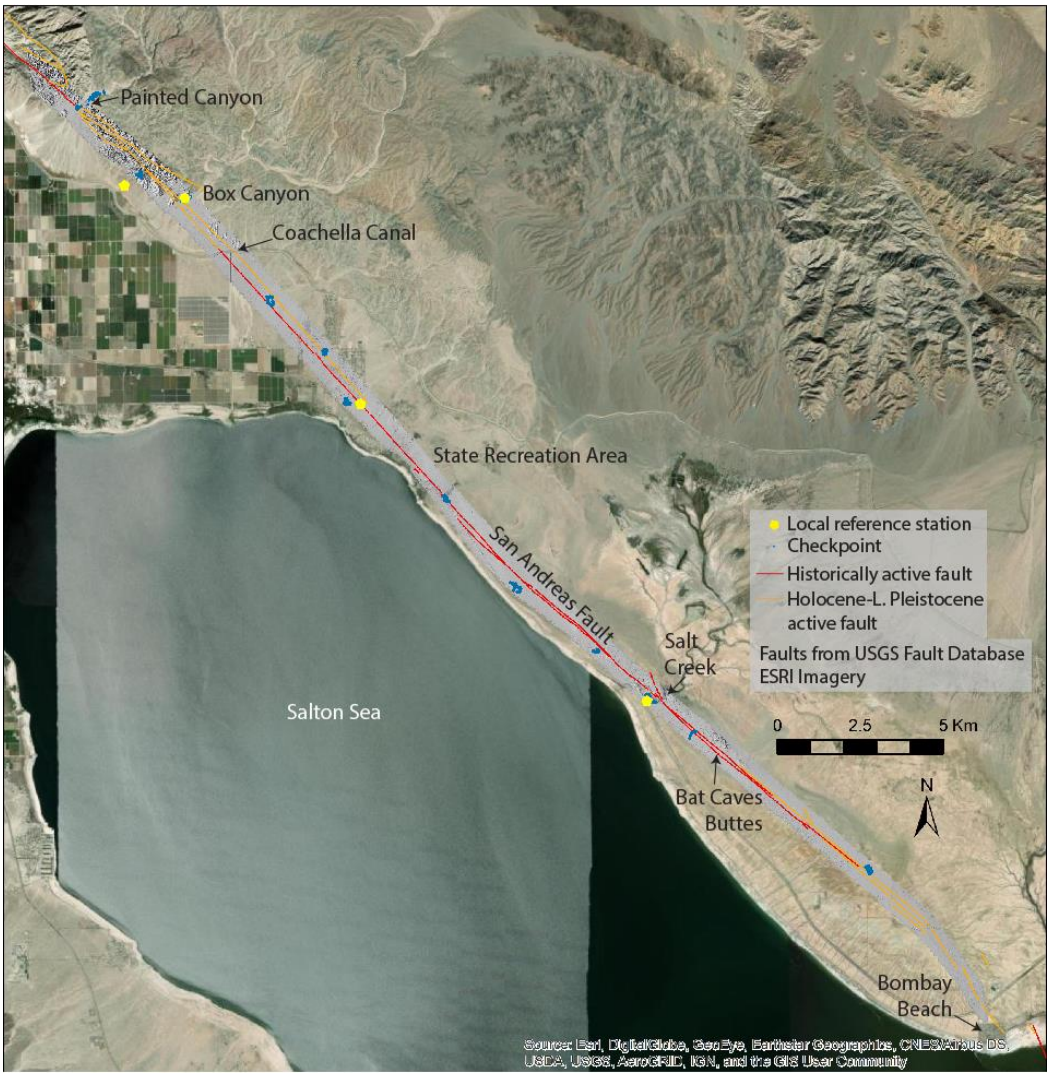

Figure 2. Map showing coverage of our sUAS topographic data set in gray, and locations of our local GNSS reference stations (yellow) and measured checkpoints (blue). Latest Pleistocene to historically active faults from the US Geological Survey Quaternary Fault and Fold Database for reference; ESRI background imagery.

Data Description (Table 1)
Reference frame: The data are in EPSG 32611, which is WGS84 UTM Zone 11 north, and ellipsoid heights. The reference stations used for georeferencing were processed in IGS2014 epoch 2020.131, so the dataset is effectively in that reference frame. See processing notes for more information on georeferencing.

1. Point cloud: 8.4 x 10^9 points. Each point has RGB attributes and all points are unclassified.
2. Digital surface model (DSM): 0.10 m pixel spacing. The DSM was rasterized from the point cloud in Agisoft Metashape (v1.7), using a 'binning' algorithm. The DSM pixel elevation is the average of the elevations of all points that lie within the pixel area.
3. Orthomosaic: 0.04 m pixel size. The orthomosaic was constructed from the aerial photographs in Agisoft Metashape. The DSM was used to orthorectify the imagery and photograph colors were blended.

Data Collection Overview
Our crew of four completed field work in approximately 3.5 days on February 15-18, 2020. Field work comprised obtaining aerial photographs and dGNSS data. We used a Sensefly eBee Plus equipped with a SODA camera and onboard dual frequency dGNSS to collect 15773 aerial photographs. We set up a local reference station each day to determine eBee camera positions and to measure checkpoints for data quality control and vertical adjustment of the final topographic model.

We generated flight plans with Sensefly eMotion software including specifying the survey area, photograph ground sample distance, and photograph overlap, with a target flight altitude of 120 m above ground level (agl). Ground sample distance averages 3.45 cm/pixel. Flight altitude sometimes slightly exceeded 120 m agl above topographic low spots in order to maintain ~120 m altitude over hills and vegetation. Overlap calculated by Agisoft Metashape is > 9x over nearly the entire study area, with exceptions primarily along the model edges. We completed a total of 22 ~ 1 hour duration flights with the eBee. Variation in natural lighting is evident in the orthomosaic particularly in areas near Bombay Beach (at the southeast end of the dataset) and northwest of Salt Creek, which were flown late in the day. Effects from the low light may also be present in the point cloud and DSM. Each day we set-up a GNSS reference station and measured checkpoints; see the georeferencing section below for more information.

Structure-from-Motion Processing
We used Agisoft Metashape Pro (v1.6 – v1.7) to produce the point cloud, DSM and orthomosaic using the following workflow: We generated the camera models and a sparse cloud (tie points) using the 'highest' setting. The models and sparse cloud were then georeferenced and optimized using camera positions generated for each photograph using the sUAS onboard dGNSS system and PPK processing (see georeferencing section below). Agisoft fit a modified Brown-Conrady camera distortion model (an a priori camera distortion model was not used). Sparse cloud points with reconstruction uncertainty greater than 10 or reprojection error greater than 0.3 were then removed incrementally in conjunction with re-optimization of the sparse cloud. The dense point cloud was generated using the 'high' setting (i.e., photos were downsampled x2). Model data parameters are summarized in Table 1. Processing was done on a cluster of five workstations equipped with 12 GPUs located at Utah Valley University's Geospatial Laboratory. Approximately 48 hours computing time was required to complete a model (i.e., camera alignment, optimization and cleaning of the sparse cloud, and generation of the dense point cloud).

Table 1. Summary of Topographic Model Parameters

Parameter	SSAF topographic model
Total points	8.43×10^9
Coverage area	34.3 km^2
Average point density	246 points/m^2
Photograph count	15773
Average GSD	0.034 m
Number of GCPs*	4*
Number of checkpoints	155
Horizontal Checkpoint RMS Error (From 28 checkpoints)	0.019 m
Vertical Checkpoint RMS Error (From 155 checkpoints)	0.033 m
DSM resolution	0.1 m
Orthomosaic resolution	0.040 m
Horizontal reference frame – point clouds, DSMs and orthomosaics	WGS UTM Zone 11 (EPSG 32611) from IGS14, epoch 2020.131
Vertical reference frame	IGS14 Ellipsoid
Field data collection date	February, 2020

* Primary data source for georeferencing is dGNSS camera positions. GSD: Ground sample distance (average spacing between adjacent photograph pixel centers), GCP: Ground control point, DSM: Digital Surface Model

The lower quality point cloud periphery was not trimmed in order to share the maximum amount of topographic data. The edges of the mapped area have lower point density and accuracy because insufficient photograph overlap is unavoidable near the boundaries of an sUAS flight, and the lack of overlap degrades the SfM point cloud. The model degradation at its periphery is evident in the DSM, particularly via derivative products such as a hillshade.

Point cloud points were not classified, and the DSM was made in Agisoft Metashape using the entire point cloud. A local gridding method was used to create the DSM, wherein the elevation of each pixel is an average of the elevation values within the pixel area. The orthomosaic was made using the DSM for orthorectification and the default mosaic blending mode in Agisoft Metashape.

Georeferencing and Accuracy

All data (point cloud, DSM, orthomosaic, and checkpoint locations) are provided in WGS84 UTM zone 11 (EPSG 32611), with ellipsoidal heights in units of meters. We processed the reference station positions, on which all georeferencing data were based, in ITRF2014 epoch 2020.131 so the data are effectively in that system and epoch. Camera positions were the primary data source for georeferencing. We used

four GCPs for georeferencing in on area, and measured 161 checkpoints. All camera positions, GCPs, and checkpoints were measured using dGNSS differenced against our reference stations.

We established a local reference station each day near the flight locations for that day. The station was a Septentrio PolaRx5 receiver paired with a Trimble Zephyr Geodetic 2 antenna on a tripod. Temporary survey markers for each reference station consisted of a hole drilled in a stable boulder and could be re-occupied. Reference station occupations ranged from 4.3 to 7.3 hours, and positions were determined using the National Geodetic Survey's Online Positioning User Service (NGS OPUS) and precise ephemeri. The reference station solutions had 0.0014-0.0064 m horizontal errors and 0.002- 0.008 m vertical errors. dGNSS processing was conducted at the Geospatial Laboratory at Utah Valley University.

The Sensefly eBee Plus incorporated a multiple frequency dGNSS system that recorded positions at 1 Hz and a time stamp for each photograph. Camera positions for the photographs were post-processed (i.e., PPK) using Sensefly/Septentrio's software and the local reference station data and position. The exception is a subset of camera positions from the southernmost flight which were post-processed against a nearby CORS station (DHLG) because accurate fixed position solutions were unavailable with our local reference station. The software calculates the camera position for each photograph by interpolating the dGNSS 1 Hz results and adjusting for the camera offset (i.e., camera position relative to the GNSS antenna phase center). These camera positions were uploaded to Agisoft. Camera position has a 0.005- 0.050 m horizontal uncertainty and a 0.010- 0.100 m vertical uncertainty.

We used four GCPs for georeferencing. GCPs consisted of markers placed on the ground and visible in sUAS photographs. We measured the GCP positions using dGNSS in kinetic mode and post-processed against the local reference station using Trimble Business Center. During the SfM processing, GCP positions were manually marked in every photograph in Agisoft Metashape prior to the sparse point cloud and camera model optimization. GCP location measurement uncertainty is approximately 0.01-0.02 m (horizontal) and 0.015- 0.04 m (vertical). An additional 0.01-0.04 cm vertical uncertainty may exist due to movement of the GCP markers caused by wind.

We measured 155 checkpoints with dGNSS (PPK) to assess DSM and point cloud accuracy. 127 checkpoints were measured on bare ground, and 28 included a marker visible in aerial photographs like the ones used for GCPs. We measured the marker position in the field and marked the visible marker position in Agisoft, as we did for the GCPs. Agisoft calculated the misfit between the measured and model-predicted marker position. The checkpoints were not used for georeferencing so they are an independent measure of model precision. The root-mean-square-error (RMSe; 1-sigma uncertainty) is 0.019 m horizontal and 0.037 m vertical for the 28 checkpoints with markers. The RMS vertical error between all 161 measured checkpoints and the DSM elevation at the checkpoints is 0.033 m. Camera positions, GCPs, and checkpoint locations were measured using the same reference stations so these errors do not account for reference station position errors, often up to 0.01 m.

The topographic model was adjusted upward by 0.018 m to remove a vertical bias relative to the measured checkpoints. The bias was the average difference between measured checkpoint elevations and elevations predicted for the checkpoint locations by the topographic model. The vertical bias likely reflects systematic error in the camera lens model. We have found similar biases in all other models that we have georeferenced with camera positions determined directly from dGNSS onboard the sUAS. The RMSerror values provided above were calculated after removal of the vertical bias.

We had dGNSS difficulties for two flights, resulting in reduced accuracy in those locations. Near the Salton Sea Recreation Area (south of North Beach, ~3708104m N, 600543 m E; ~33.5078 N, 115.9175 W), we used camera positions from autonomous GNSS solutions and four GCPs located with dGNSS for georeferencing. Vertical error here is likely up to ~0.3- 0.5 m. At the far eastern edge of the surveyed area we obtained dGNSS positions for the easternmost row of photographs, but for 173 camera positions just to the west of the eastern edge we did not obtain accurate dGNSS. Thus, the eastern most ~500 m of coverage in that area also has vertical error of ~0.3 m. In both of these problem areas, the inaccuracy is due primarily to long wavelength warping, so topographic patterns are still well imaged and precision of positions across distances of meters to 10's of meters is likely to remain very good.

Although we have endeavored to minimize and quantify error in the data set, no guarantee of accuracy is given nor implied. DSM and point cloud error likely varies across the data set.

For additional information please contact Michael Bunds (michael.bunds@uvu.edu).

References Cited

Bevis, M. and Hudnut, K. (2005): B4 Lidar Project: Airborne Laser Swath Mapping (ALSM) survey of the San Andreas Fault (SAF) system of central and southern California, including the Banning segment of the SAF and the San Jacinto fault system. National Center for Airborne Laser Mapping (NCALM), U.S. Geological Survey, the Ohio State University, and the Southern California Integrated GPS Project. Distributed by OpenTopography. https://doi.org/10.5066/F7TQ5ZQ6

Field et al., Jordan, T.H., Page, M.T., Milner, K.R., Shaw, B.E., Dawson, T.E., Biasi, G.P., Parson, T., Hardebeck, J.L., Michael, A.J., Weldon, R.J., Powers, P.M., Johnson, K.M,, Zeng, Y., Felzer, K.R., Elst, N., Madden, C., Arrowsmith, R., Werner, M., and Thatcher, W.R., 2017, A Synoptic View of the Third Uniform California Earthquake Rupture Forecast (UCERF3), Seismological Research Letters, v88, n. 5, pp. 1259-1267, https://doi.org/10.1785/0220170045

U.S. Geological Survey and California Geological Survey, Quaternary fault and fold database for the United States, accessed August, 2020, at *https://www.usgs.gov/natural-hazards/earthquake-hazards/faults*.

Acknowledgements

This project was supported by the Southern California Earthquake Center (SCEC) awards 19123 and 21107 to Scott, and awards to Bunds from Utah Valley University's Office of Engaged Learning and College of Science Scholarly Activities Committee. We thank Tony Nwabuba for able IT support at UVU, and we gratefully acknowledge a GPU Grant from NVIDIA and the support of Sensefly's educational pricing program.